Planet. Space Sci., Vol. 37, No. 10, pp. 1227–1247, 1989
Printed in Great Britain.

0032-0633/89 $3.00+0.00
Pergamon Press plc

SHOCKLIKE BEHAVIOUR EXHIBITED AT EARLY TIMES BY THE *AMPTE* SOLAR WIND/MAGNETOSHEATH RELEASES

S. C. CHAPMAN*
Astronomy Unit, Queen Mary College, London E1 4NS, U.K.

(*Received in final form* 12 *May* 1989)

Abstract—The boundary layer structures that form at early times upstream of an *AMPTE* release in the solar wind or magnetosheath flow are examined using one dimensional hybrid simulations. (This is appropriate since the releases generate perturbations to the ambient flow on scales less than, or approaching the ion gyroscales, but far in excess of the electron gyroscales.) This work is an extension of a previous study of the solar wind releases (Chapman and Schwartz, 1987, *J. geophys. Res.* **92**, 11,059), and is also the first study appropriate for magnetosheath conditions. Just upstream of the release ion cloud and associated diamagnetic cavity a region of enhanced magnetic field forms, bounded on either side by small scale boundary structures, which act to transfer momentum from the oncoming flow to the bulk of the release ions, located within the cavity. On the downstream side, at the cavity edge, a quasi-steady "snowplough" type structure evolves in which the electron and magnetic pressure gradients act to accelerate release ions within the vicinity downstream. On the upstream side, the transition between the incident flow and that in the compression region has associated ion kinetics similar to those found at supercritical, quasi-perpendicular shock transitions. For a solar wind release the upstream boundary remains approximately at rest in the release frame, but for a magnetosheath release it rapidly moves upstream, implying an initial disturbance to the incident flow on a much larger scale. In this case, incident protons that reflect off the upstream boundary may after gyrating in the upstream magnetic field return to be transmitted downstream, rather than being lost, as their transverse motion no longer exceeds the spatial dimensions of the release cloud. A steady state then evolves so that Rankine Hugoniot relations can be used to deduce the properties of the upstream boundary layer analytically. These properties are effectively constrained by the behaviour of the snowplough boundary, since the flow speed downstream of the upstream boundary layer (i.e. in the magnetic compression region) is just approximately the speed at which the snowplough propagates, which in turn can be deduced approximately from a simple equation of motion for the snowplough boundary.

1. INTRODUCTION

As part of the *AMPTE* (Active Magnetospheric Particle Tracer Explorers) mission (Krimigis *et al.*, 1982), slowly expanding clouds of photoionizing lithium and barium neutrals were released in the solar wind and magnetosheath. At a sufficiently early stage in the interaction, the ion clouds thus produced were sufficiently mass dense to strongly perturb the ambient flow, and it is this aspect of the release behaviour that will be under discussion here. Initially, in the central region of the release cloud, the number density of release electrons is sufficiently high to produce a diamagnetic cavity in the ambient electromagnetic fields. This field zero region is observed at the spacecraft from which the releases were performed, the IRM (Ion Release Module) and which at early times was located at the release cloud centre (e.g. Lühr *et al.*, 1986a,b). A second spacecraft, the *UKS* (United Kingdom Subsatellite) which was in an orbit close to that of the IRM, did not become immersed in the diamagnetic cavity associated with the solar wind events, so that the separation of the two spacecraft (of ~ 30 km for the Li, and ~ 170 km for the Ba releases, respectively) gives an indication of the scale size of the interaction region. The *UKS* was no longer operational at the time of the single Ba release in the magnetosheath, but ground-based optical observations (M. Mendillo, private communication) suggested a dense release ion cloud on a similar scale to that seen in the solar wind event.

These estimates of the spatial scale of the interaction region, along with temporal scales suggested by the length of time for which the cavity is seen by the *IRM* (i.e. ~ 7 s for Li, and ~ 80 s for Ba), all imply scales which are smaller than, or of the order of the Larmor scales of both the oncoming protons and release ions which have "picked up" (i.e. gained momentum from) the oncoming flow. The electron Larmor scales are on the other hand expected to be small compared with the release cloud scales, leading to a "hybrid" description in which the ions are treated kinetically (or at least, as a multifluid) whereas a single massless fluid is used to describe the electron behaviour (see e.g. Chapman and Dunlop, 1986; Chapman and Schwartz, 1987).

* Now at Geophysics Institute, Kyoto University, Sakyo-ku, Kyoto 606, Japan.

Previous authors, such as Haerendel *et al.* (1986), Papadopolous *et al.* (1986), Cheng (1987), Lui *et al.* (1986), Brecht and Thomas (1987) and Chapman (1989), have discussed the global transfer of momentum to the release ion cloud as a whole, in order to explain the observed cloud motion. Instead here we concentrate on the details of the interaction which occur locally, and which are revealed by resolving the interaction on hybrid scales. However, it has already been shown (Chapman and Schwartz, 1987; Chapman, 1989) that these phenomena, occurring locally, may be expected to be a controlling factor in the global interaction.

This paper is primarily a study of the "local" interaction in terms of simple properties of supercritical, quasiperpendicular shock transitions. In a previous study, one dimensional hybrid code simulations were performed (Chapman and Schwartz, 1987) for the case of a release in the solar wind. Here we present a further, more detailed analysis of those results, and of new results obtained for the case of a release in the magnetosheath. Key features are found to be in common to both cases; these are introduced in the next section. These features are interpreted in terms of the ion kinetics and bulk plasma behaviour of supercritical, quasiperpendicular shock transitions, that have been revealed by both hybrid code studies and *in situ* observations. Sections 3 and 4 contain the discussion of the simulation results for the solar wind and magnetosheath events.

2. "LOCAL" INTERACTION: OVERALL BEHAVIOUR

We will first describe the overall features of the "local" momentum exchange process that are found to be in common with both the solar wind and magnetosheath events, before examining each event in turn in detail. The approach here is to treat the ions kinetically, so that we can represent the interaction of several ion fluids, each with different properties, each of the different species of the oncoming protons and release ions generally being comprised of more than one fluid. The electrons, on the other hand, are represented by a single, massless, charge neutralizing fluid, regardless of their origin. The system of equations that are solved in the hybrid code are described in Chapman and Schwartz (1987). Here we can summarise the various forces acting on the ions by examining the momentum equation of the αth ion species:

$$\rho_\alpha \frac{\partial \mathbf{v}_\alpha}{\partial t} + \rho_\alpha \mathbf{v}_\alpha \cdot \nabla \mathbf{v}_\alpha = e n_\alpha \left(\mathbf{v}_\alpha - \frac{1}{n} \sum_{\alpha'} n_{\alpha'} \mathbf{v}_{\alpha'} \right) \times \mathbf{B} - \frac{n_\alpha}{n} \nabla \cdot (\mathbf{T} + \mathbf{P}_e) - \nabla \cdot \mathbf{P}_\alpha \quad (1)$$

where the ion bulk moments of the fluid as a whole are defined in the centre of mass frame as

$$n = n_i = \sum_\alpha n_\alpha \quad (2)$$

$$\mathbf{v}_i = \frac{\sum_\alpha n_\alpha m_\alpha \mathbf{v}_\alpha}{\sum_\alpha n_\alpha m_\alpha} \quad (3)$$

$$\mathbf{P}_i = \sum_\alpha (\mathbf{P}_\alpha + m_\alpha n_\alpha \mathbf{v}_\alpha \mathbf{v}_\alpha) - mn\mathbf{v}\mathbf{v}. \quad (4)$$

The single massless electron fluid momentum equation;

$$m_e \frac{d\mathbf{v}_e}{dt} = -e(\mathbf{E} + \mathbf{v}_e \times \mathbf{B}) - \frac{\nabla \cdot \mathbf{P}_e}{n} + e\eta \mathbf{J} \quad (5)$$

in the limit

$$m_e \frac{d\mathbf{v}_e}{dt} \to 0$$

has been used to substitute for the electric field on the right hand side of (1). All symbols have their usual meanings, and $\mathbf{T}$ is the Maxwell stress tensor (i.e. $\nabla \cdot \mathbf{T} = \mathbf{j} \times \mathbf{B}$). The first term on the right hand side of (1) is then of the form $\mathbf{U}_\alpha \times \mathbf{B}$, where $\mathbf{U}_\alpha$ is the difference in velocity between the αth fluid and the centre of charge of the entire plasma. The "$\mathbf{U}_\alpha \times \mathbf{B}$" term refers to a process by which momentum is locally (on scales $< R_{gi}$) transferred between different ion species. This can be most easily envisaged if we consider a plasma with two distinct ion fluids α and β. Considering only the "$\mathbf{U}_\alpha \times \mathbf{B}$" term on the right-hand side of (1) we have:

$$m_\alpha \frac{D\mathbf{v}_\alpha}{Dt} = \frac{n_\beta}{n_\alpha + n_\beta} (\mathbf{v}_\alpha - \mathbf{v}_\beta) \times \mathbf{B} + \ldots \quad (6)$$

Thus photoionizing a large quantity of release ions at rest in the oncoming proton flow that is moving initially at velocity $\mathbf{v}_p$ will, in the regions outside of the diamagnetic cavity, cause the proton flow to be deflected initially in the $\mathbf{v}_p \times \mathbf{B}$ direction, the release ions being initially accelerated in the $-\mathbf{v}_p \times \mathbf{B}$ direction in order to conserve momentum (see Chapman and Dunlop, 1985; Chapman and Schwartz, 1987). Similar behaviour would be expected if the oncoming protons were to instead move into a region of comparatively slowed proton flow. This term then represents a transfer of momentum between different ion fluids which exhibit distinct behaviour, the term vanishing when (1) is summed over α.

In one dimensional geometry, the $\mathbf{U}_\alpha \times \mathbf{B}$ term is the only term in the right-hand side of (1) that has a non-

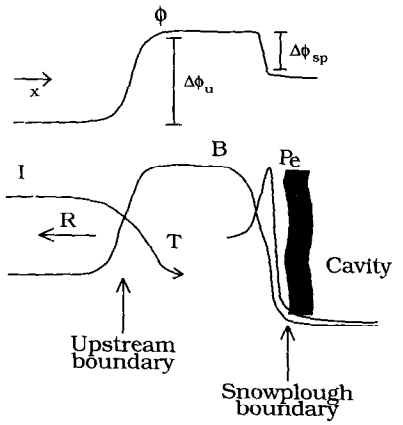

FIG. 1(a). A SKETCH OF THE VARIATION OF THE ELECTRON AND MAGNETIC PRESSURES AND THE POTENTIAL WITH DISTANCE x ALONG THE COMPUTATIONAL BOX.
The snowploughed release ions (shaded region) move to the right (downstream) with the snowplough boundary structure which accelerates them. The incident protons (I) enter at the left-hand side and are decelerated by the upstream boundary structure. Most are transmitted (T), but some are reflected (R) on this first interaction.

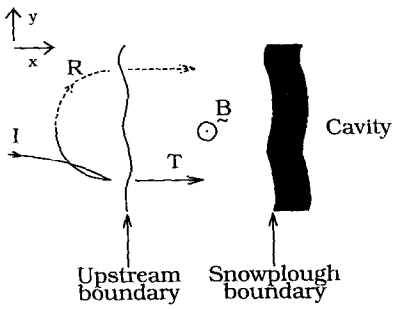

FIG. 1(b). A SKETCH OF THE ION KINETICS IN THE PLANE PERPENDICULAR TO **B**.
The snowploughed release ions (shaded region) move downstream "en masse". The incident protons (I) are deflected in the $\mathbf{U}_x \times \mathbf{B}$ direction (where $\mathbf{U}_x$ is their velocity relative to the plasma centre of charge) as they move into regions occupied by distinct populations moving at different relative velocities. On interacting with the upstream boundary layer most are slowed and transmitted (T), the remainder are reflected (R) and gyrate in the upstream magnetic field. If the obstacle has sufficient transverse extent the reflecting–gyrating ions can return (dashed line) to the upstream boundary layer to be transmitted downstream.

zero component acting transverse to the direction of variation (hereafter the $\hat{\mathbf{x}}$ direction). The remaining terms, representing gradients in magnetic, ion and electron pressure, are constrained to act only along the $\hat{\mathbf{x}}$ direction of the one dimensional simulation "box". The overall features of this longitudinal (i.e. along $\hat{\mathbf{x}}$) momentum exchange between the various fluids are sketched in Fig. 1a, and the ion kinetics in the transverse, or $\hat{\mathbf{y}}$ direction (i.e. in the plane perpendicular to the magnetic field), in Fig. 1b. In this simple description $\mathbf{B} = B\hat{\mathbf{z}}$ everywhere, consistent with the simulation results. The figures, which represent a plot along the simulation box, show only those features common to both solar wind and magnetosheath releases. The lower sketch in Fig. 1a, shows the variation with x of the magnetic and the electron pressures, the upper sketch, the potential, the latter being defined in the rest frame of the simulation (and of the release) by the $\hat{\mathbf{x}}$-component of the electric field $E_x = -\nabla\phi$. This is given by the $\hat{\mathbf{x}}$-component of the massless electron momentum equation, (5), which along with $\nabla \times \mathbf{B} = \mu_0 \mathbf{J}$ gives:

$$enE_x = -en\nabla\phi = -j_{iy}B - \nabla\left(P_e + \frac{B^2}{2\mu_0}\right)$$

$$\approx -\nabla\left(P_e + \frac{B^2}{2\mu_0}\right) \quad (7)$$

if $j_{iy} \ll j_{ey}$.

As generally $j_{iy} < j_{ey}$ in the results here, the form of ϕ follows that of the electron and magnetic pressures. The incident magnetized proton flow (labelled I) enters the box on the left, and the slowly moving ($v = 1-2$ km s^{-1}) release ions within the diamagnetic cavity enter on the right. The quasi-steady boundary structure that forms between these two regions acts to transfer $\hat{\mathbf{x}}$ directed momentum between the protons and cavity associated release ions. Under the above approximation this is achieved directly via the x electric field from equation (7), since

$$m_i \frac{dv_{ix}}{dt} = e(E_x + v_{iy}B) = -\frac{1}{n}\nabla\left(P_e + \frac{B^2}{2\mu_0}\right) \quad (8)$$

$$\approx eE_x = -e\nabla\phi \quad (9)$$

if $j_{iy} \ll j_{ey}$.

The release ion population not shown here, that is created in regions where the magnetic field is not zero, will also gain momentum via the $\mathbf{U}_x \times \mathbf{B}$ process, deflecting the oncoming flow. The bulk of the release ions however, that are associated with the cavity, are accelerated to the right in the $+\hat{\mathbf{x}}$ direction only, by the combined magnetic and electron pressure gradients that exist at the cavity edge. This population (indicated by the shaded region) is gathered up "en masse" by a "snowplough" type process, and move to the right at the same speed v_p as the snowplough field structures in the vicinity without significant transverse displacement. The potential jump at the snowplough boundary $\Delta\phi_{sp}$ is hence just sufficient to

accelerate these release ions to the snowplough speed. Details of the dynamics of the snowplough boundary found for releases in the solar wind have been addressed previously by Chapman and Schwartz (1987) and will therefore not be discussed further here. We shall see that the same snowplough boundary layer structure also evolves in the case of a magnetosheath release.

We concentrate here on the behaviour of the upstream boundary also shown in the figure. In all cases the majority of the incident protons are slowed, but transmitted (marked T) through the boundary layer on their first interaction with it. The remaining fraction (marked R) is reflected back upstream. This provides $+\hat{\mathbf{x}}$ directed momentum which is ultimately transmitted to the "snowploughed" release ions. Since $j_{iy} \ll j_{ey}$, the potential gradient ($-\hat{\mathbf{x}}$ directed electric field) required to slow the protons arises principally from enhancements in the magnetic and electron pressures. Under this approximation the expression (9) implies that the change in kinetic energy of the protons as they pass through the boundary layer is just given by the potential jump $\Delta\phi_u$ that they encounter, provided that this change in kinetic energy is calculated in the rest frame of the boundary layer. It is the structure and dynamics of this upstream boundary layer that at early times differs substantially between a solar wind and magnetosheath event, and that is to be interpreted here with reference to simple properties of collisionless, quasiperpendicular shock transitions.

Two aspects of shock structure are used here to characterize the upstream boundary layer structure; the details of the ion kinetics and the behaviour of the plasma bulk properties. Both are given by the hybrid representation. The key features of the ion kinetics are shown in Fig. 1b, a sketch of the projection of the trajectories of individual ions on the plane perpendicular to **B** (i.e. in the x, y plane) with the $\hat{\mathbf{x}}$ direction oriented as in Fig. 1a, for comparison. As the incident proton population (marked I), moves in from the left, it drifts transverse to the boundary layer in the $\mathbf{U}_\alpha \times \mathbf{B}$ direction as it encounters a region where the bulk flow speed has dropped due to the presence of release ions if they are photoionized in this region, and/or protons which reflect off the upstream boundary. In a simple picture, with a structure of infinite extent in the transverse directions, the oncoming protons divide into two populations, one being transmitted directly through the boundary layer (marked T) losing momentum, the other being reflected (marked R) to gyrate in the upstream magnetic field and ultimately return to the boundary layer, to be transmitted into the region of compressed magnetic field downstream, but with a transverse displacement of about twice the ion gyroradius in the upstream **B**-field. In a steady state, one dimensional supercritical shock structure these reflecting gyrating ions are known to play an essential role in providing the increase in ion pressure across the shock (e.g. Leroy, 1983; Schwartz *et al.*, 1983). The discovery of reflecting ions in the case of the *AMPTE* releases, in both the one dimensional hybrid simulations discussed here, and in the observations of the barium releases (Dunlop *et al.*, 1987, 1989) provides the rationale for examining the structure of the upstream boundary layer in terms of the behaviour seen at shock transitions.

The key difference between a planar (i.e. one dimensional) shock transition and the upstream boundary layer formed during the early stages of a release lies in the finite transverse dimension of the release ion cloud (i.e. in the $\hat{\mathbf{y}}$ direction). As a consequence, the reflecting–gyrating protons may have sufficiently large gyroradii in the upstream field that they do not return to traverse the upstream boundary layer. This will clearly be the case in the solar wind, for example, where the approximately specularly reflected protons with $v \simeq 500$ km s^{-1} in a 10 nT field will have a transverse displacement of $2r_\Omega^i \simeq 1000$ km, which is far in excess of the few hundred kilometre diameter of the structure associated with a barium release in the solar wind. Whether or not this is also the case in the magnetosheath will be addressed later here.

If the reflected protons are expected to "miss" the release cloud, then in the one dimensional model they represent a sink of particles and it is appropriate to remove them from the simulation, as was done previously in the study of the solar wind release (Chapman and Schwartz, 1987). The resulting structure will not achieve a steady state (but may become quasi-steady). However if the protons do re-enter the boundary layer, the resulting structure may instead evolve into a steady state more closely resembling a shock transition. In this case, Rankine Hugoniot relations will then be satisfied on some sufficiently large spatial scale, and can be used to predict the downstream bulk parameters (i.e. in the compression region, upstream of the snowplough) in terms of the upstream parameters, or vice versa. We can deduce whether the boundary is in steady state by rearranging the multifluid moment equations to give conservation relations (e.g. Boyd and Sanderson, 1970). In steady state (i.e. no sources or sinks of particles) this yields quantities conserved throughout the layer:

$$M_T = \sum_\alpha \rho_\alpha v_{\alpha x} \tag{10}$$

$$P_T = \sum_\alpha (\rho_\alpha v_{\alpha x}^2 + P_\alpha) + \frac{B^2}{2\mu_0} + P_e \tag{11}$$

$$\varepsilon_T = \frac{E_y B_z}{\mu_0} + \tfrac{5}{2} v_{ex} P_e + \sum_\alpha (\tfrac{5}{2} v_{\alpha x} P_\alpha + \tfrac{1}{2} \rho_\alpha v_{\alpha x}^3) \quad (12)$$

where the individual fluid pressures have been assumed to be isotropic, and the heat flux has been neglected. Steady state also requires E_y to be constant in this one dimensional description, since $\nabla \times \mathbf{E} = 0$, so that far upstream and downstream of the boundary layer, where $\mu_0 J_y = \partial B/\partial x = 0$, the $\hat{y}$-component of the massless electron fluid momentum equation gives conservation of magnetic flux:

$$E_y = v_{ex} B. \quad (13)$$

If the plasma may be treated as a single ion fluid and a single electron fluid in the regions far upstream and downstream of the boundary layer, all of the summations over α in the above expressions are known. In this case equations (10)–(13) directly yield the Rankine Hugoniot jump conditions (e.g. Tidman and Krall, 1971) given also that $v_{ix} = v_{ex} = v_x$ as a consequence of quasi-neutrality in one dimensional geometry. In any case, we shall use conservation of M_T, P_T, ε_T and E_y [equations (10)–(13)] across the boundary layer to investigate whether it is in steady state. Also, conservation of P_T [equation (11)] alone has important consequences concerning predictions of the snowplough motion, since this leads to an approximate equation of motion of the snowplough boundary and associated release ions (Chapman and Schwartz, 1987; Chapman, 1989).

3. RESULTS

3.1. *Solar wind release*

Here we discuss the results of a simulation presented in Chapman and Schwartz (1987). Rather than reiterate the results of that study here we will, after briefly introducing the simulation parameters, present the findings of the analysis here in Fig. 2. Briefly, the simulation box shown in the figure represents 250 km and is divided into 400 cells, giving an effective resolution comparable with c/ω_{pe} (the limit of resolution of the massless electron fluid description). More than $\sim 7 \times 10^4$ particles are used in the simulation. Typical solar wind parameters used are $M_{Asw} \approx 5$, $\beta_p \approx 0.1$ ($T_e = T_p = 5$ eV), the solar wind enters on the left-hand side at a number density of 5 cm^{-3} and initially pervades the box. The release is represented by a cold beam of Li^+ at a density of $n_{r0} = 100$ cm^{-3} entering at the right-hand side of the box (at a speed $v_r = -2$ km s^{-1}), where the magnetic field is zero. The initial Li^+ density falls away as we move upstream, or to the left of the box, as $n_{r0}(1+\tanh(x-x_0)/l)$,

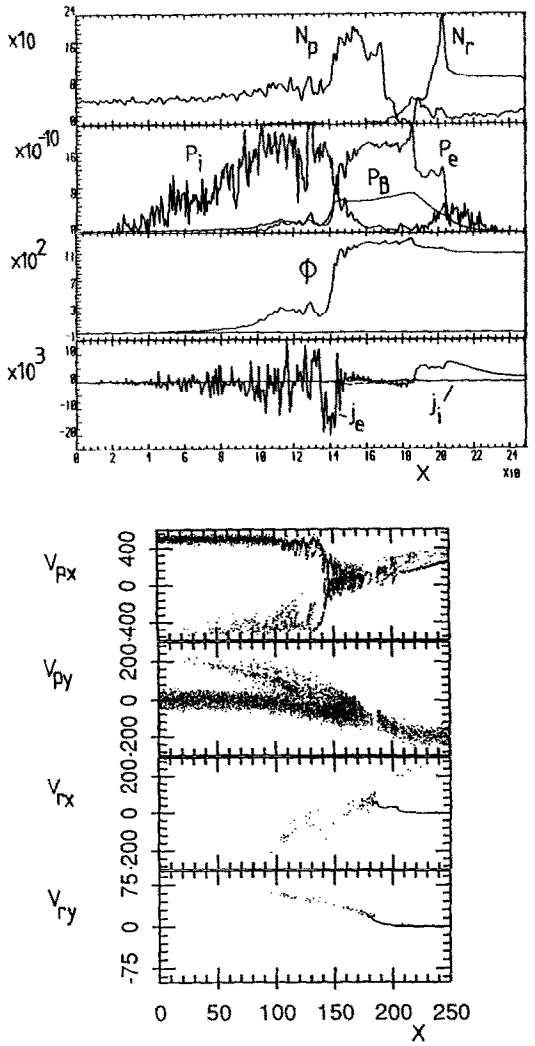

FIG. 2. THE QUASI-STEADY BOUNDARY STRUCTURE THAT EVOLVES IN THE CASE OF A RELEASE IN THE SOLAR WIND. The upper four panels show, from top to bottom, the release ion and proton number densities (N_p multiplied by a factor of 8), the electron, ion and magnetic pressures, the potential, and the electron and ion contributions to the current. The lower four panels show the locations of the computational particles in phase space. All quantities are plotted against distance along the computational box, x, and are in SI units.

the magnetic field rising on the same scale to its ambient value of 10 nT at the left-hand side, and with the tanh function centred on $x_0 = 180$ km. Here, as in the magnetosheath results to be presented later, the half thickness $l = 20$ km, this represents the spatial region which at early times may become pervaded by the photoionizing release neutral cloud which expands at $v \approx$ few km s^{-1}. The computational par-

ticles are free to exit the box at both boundaries. The magnetic field is initially wholly in the $\hat{\mathbf{z}}$ direction and remains so throughout the simulation (consistent with conservation of helicity). The results are found to be qualitatively independent of the mass and number density chosen for the release ions, so that the overall behaviour revealed by the analysis here should be applicable to both the Li^+ and the Ba^+ releases. The evolution of the initial conditions into the quasi-steady configuration sketched in Fig. 1 is documented in Chapman and Schwartz (1987). Studies using different masses and densities for the release ion cloud imply that this evolution time would be less than, or of the order of a second for a Li^+ release, and of the order of a few seconds for a Ba^+ release, that is, on timescales short in comparison with the observed cavity lifetimes.

The overall morphology of this quasi-steady boundary layer is shown in the top panel of Fig. 2, which is a plot of the proton and release ion number densities (per cubic centimetre) vs distance along the simulation box (along $\hat{x}$) in kilometres. For clarity the proton number density has been multiplied by a factor of 8. The location of the "snowploughed" release ions (see Fig. 1) can immediately be identified by the spike in the release ion number density, at $x = 203$ km. The upstream boundary layer, under discussion here, is located where the proton number density increases sharply, at $x = 144$ km, as a result of slowing the oncoming proton flow. The ion, electron and magnetic pressures are shown in the second panel. At the snowplough boundary, we can see the magnetic and electron pressure gradients which act to accelerate the snowplough release ions. The upstream boundary is characterized by a sharp fall in the ion pressure (which is enhanced upstream) and a rise in the electron and magnetic pressures. The next two panels show the potential, and the total ion (dashed line) and electron (solid line) contributions to the current. The ion current can be seen to remain small in comparison with the electron current at the boundaries where the pressure gradients are large, so as we expect from equation (7), the sharp gradients in the potential coincide with those in the magnetic and electron pressure profiles.

The jump in the potential at the upstream boundary of ~ 1300 V is just that required to slow the oncoming protons, to a good approximation, i.e. $e\Delta\phi \approx \frac{1}{2}m_p(v_u^2 - v_d^2) \simeq 1280$ eV (where v_u and v_d are the x-components of the proton velocity upstream and downstream of the upstream boundary, respectively). This is consistent with $j_{iy} \ll j_{ey}$ and the upstream boundary layer being approximately at rest in the simulation frame, i.e. the frame in which we observe the change in kinetic energy of the ions. The proton and release ion dynamics can be seen in the lower four panels of the plot, which show the x and y velocities of individual computational particles plotted vs distance along the box, x. In the $\hat{\mathbf{y}}$ direction, the oncoming protons and release ions exchange momentum via the $\mathbf{U}_\alpha \times \mathbf{B}$ mechanism [see equation (6)] in the regions where the magnetic field is non-zero, both upstream and downstream of the upstream boundary. In the vicinity of the snowplough boundary, however, momentum exchange is wholly in the $\hat{x}$ direction, the only exception being the small population of release ions ejected from the boundary structure at relatively high downstream speed.

The bulk of the oncoming protons are decelerated in the $+\hat{\mathbf{x}}$ direction as they cross the upstream boundary, without significant increase in ion pressure. The downstream speed of this population is approximately just that of the snowplough structure that is moving steadily to the right of the box. A small fraction (about 8%) of the protons do not cross the upstream boundary however, instead, being reflected, they begin to gyrate in the upstream magnetic field. This population acts to enhance the total ion pressure just upstream of the upstream boundary, since the plasma as a whole is now effectively comprised of two oppositely directed beams [see equation (4)]. If the release boundary were an infinite planar structure, the reflected protons would ultimately return to be transmitted, increasing in the net ion pressure downstream. As the extent of the release cloud in the $\hat{\mathbf{y}}$ direction, ~ 100 km at most (i.e. for a Ba release), is less than the gyroradius of the reflecting protons $R_g \approx v_u/\Omega_u \approx 1000$ km, they do not return to traverse the boundary layer. This y displacement of the reflecting–gyrating protons is significantly larger than the y motion (e.g. gyromotion) of any other population in the simulation (the oncoming protons in the upstream 10 nT field have $R_{gi} \simeq 30$ km, for example) so that we have simply removed this population from the simulation when they have moved in the $\hat{\mathbf{y}}$ direction a distance significantly greater than a release dimension.

We can make a more quantitative assessment of the properties of these reflecting–gyrating ions, in terms of those produced by 1-D hybrid code simulations of supercritical shocks. In a study in the high Mach number regime (i.e. for conditions appropriate for a solar wind release) Burgess *et al.* (1989) have shown that the reflecting gyrating population tends to originate from the part of the incident proton distribution with large thermal speeds (large velocities in the rest frame of the incident proton flow). Figure 3 shows a histogram of the reflected computational particles from the solar wind release simulation (including

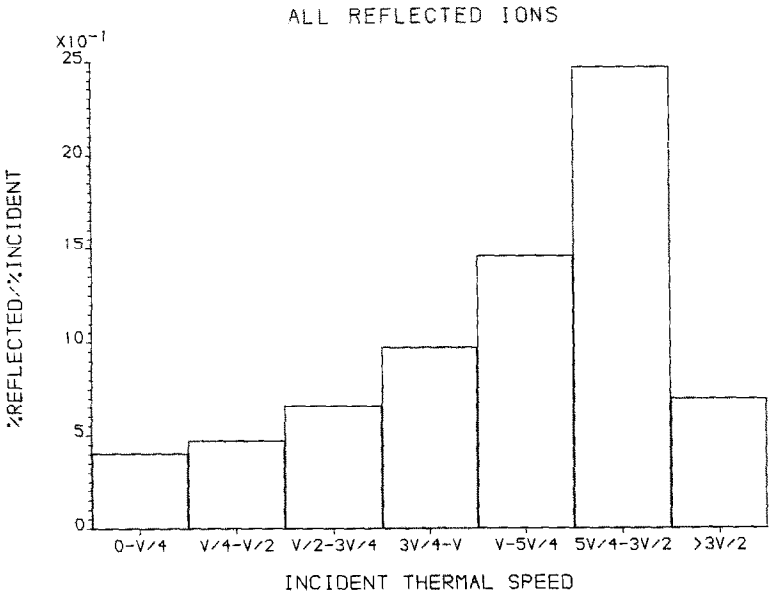

FIG. 3. THE REFLECTING–GYRATING COMPUTATIONAL PARTICLES FROM THE SOLAR WIND RELEASE SIMULATION ARE BINNED ACCORDING TO THEIR INITIAL THERMAL SPEEDS WITH WHICH THEY ENTER THE COMPUTATIONAL BOX.

The range of each bin is expressed in terms of the thermal speed associated with the temperature of the initial distribution. The number of reflecting–gyrating computational particles in each bin is expressed as a percentage of the total number reflected, which has then been normalized to the percentage of the initial distribution lying in each bin.

those removed from the simulation), binned according to their initial thermal speeds with which they were introduced into the computational box. The range of each bin is expressed in terms of the thermal speed associated with the temperature of the initial distribution, i.e. $\frac{1}{2}mv^2 = \frac{1}{2}kT_p$. The number of reflecting–gyrating computational particles in each bin is expressed as a percentage of the total number of reflected computational particles, which has then been normalized to the percentage of the initial distribution within that range of thermal speed. A bias towards the higher thermal speeds is clearly evident, with a factor of ~ 5 difference between the lowest and the higher ranges of incident thermal speed. This suggests that to some extent, the ion kinetics at the upstream boundary layer are in this case similar to those exhibited by one dimensional hybrid code studies of shock transitions.

We now move on to discuss the behaviour of the bulk plasma parameters. The conserved quantities given by equations (10)–(12) for the simulation results shown in Fig. 2 are shown in Fig. 4. The top panel shows the ion, electron and magnetic pressures, so that the location of the upstream and snowplough boundaries can be readily identified. The remaining panels, from top to bottom, show (normalized) B/ρ, M_T, P_T and ε_T. Equation (13) has been used to obtain B/ρ and ε_T, so that even in steady state we might only expect these to be constant upstream and downstream of the boundary layer. A plot of a conserved quantity that is velocity independent, such as B/ρ, is useful to indicate if the upstream boundary layer is in steady state, whether or not it is at rest in the simulation frame. We can see from the plots that this is not the case, the only quantity approximately conserved across the upstream boundary layer being the momentum flux P_T.

Conservation of momentum flux has two important consequences. First, this suggests that the upstream momentum flux $\rho_u v_u^2$ is simply related to that of the snowploughed release ions $\rho_R v_R^2$, since there is no significant loss of $\hat{\mathbf{x}}$ directed momentum flux across the upstream boundary in between. This yields a simple equation for the snowplough motion which can be used to predict the bulk motion of the actual release clouds (Chapman, 1989). Second, the simulation results suggest that the proton speed just downstream of the upstream boundary is approximately the snowplough speed, which in turn is just specified from the simple snowplough equations of motion and

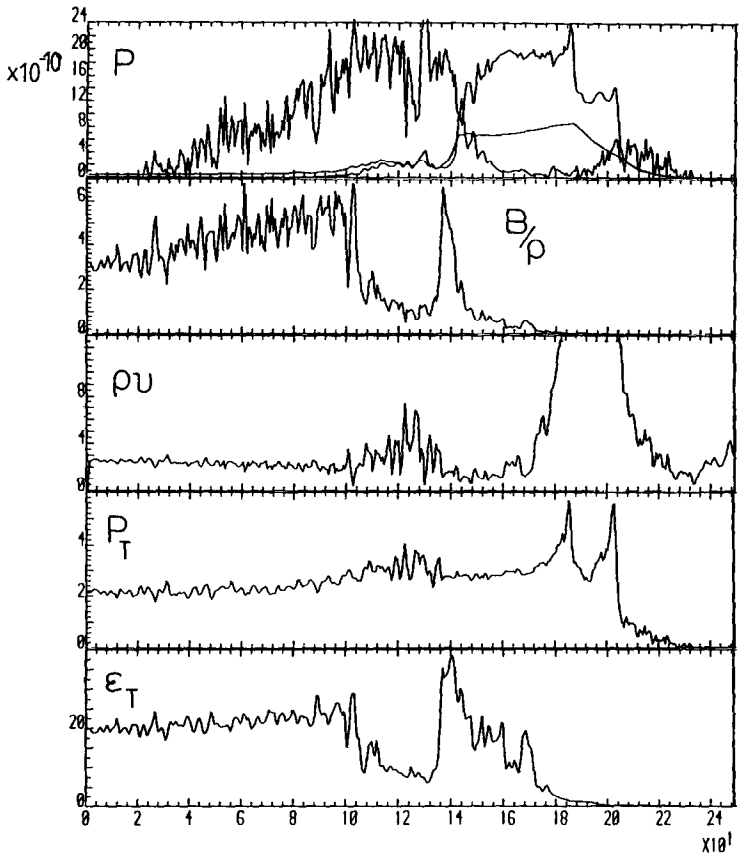

FIG. 4. THE "CONSERVED QUANTITIES" B/ρ, M_T, P_T AND ε_T (DEFINED IN THE TEXT) ARE SHOWN PLOTTED VS DISTANCE ALONG THE COMPUTATIONAL BOX x FOR THE SOLAR WIND RELEASE RESULTS SHOWN IN FIG. 2. The top panel shows the electron, magnetic and ion pressures, enabling the location of the upstream and snowplough boundaries to be identified. All quantities are in normalized units (except the pressures).

the known momentum fluxes of the incident protons and the release ion population within the cavity. It has already been verified for these results (Chapman and Schwartz, 1987) that the snowplough speed found in the simulation is in good agreement with that predicted by the snowplough equation of motion.

The sharp fluctuations in the other conserved quantities both upstream and downstream of the upstream boundary layer can be attributed to the presence of release ions in the oncoming flow, as well as the sink of reflecting–gyrating protons. On timescales much shorter than the gyroscales of the release ions, the momentum and energy exchange between the release ions and the oncoming protons in the regions of non-zero magnetic field must proceed in a strongly time dependent way, resulting in non-steady behaviour.

3.2. *Magnetosheath release*

As the single Ba^+ release in the magnetosheath was sited in the flank, where ambient flow conditions were close to supermagnetosonic, we will discuss results of simulations with parameters chosen to as closely as possible represent a release in both slightly super- and submagnetosonic flow conditions. For the purposes of comparison, these studies have most parameters in common. For the results shown here the simulation box is now 1500 km in extent, divided into 600 cells so that the spatial resolution, although larger than in the solar wind simulations, remains comparable with c/ω_{pe} to within a factor of 10. Simulations at higher resolution (i.e. up to c/ω_{pe}) have been performed to verify that the results presented here are independent of this choice of cell size. A larger number of computational particles, $\sim 5\times 10^5$, was required in order to maintain a good statistical representation of the higher temperature magnetosheath flow.

The release population is again given by $n_{r0}(1+\tanh(x-x_0)/l)$ as in the solar wind release simulation, with $x_0 = 1250$ km. The number density at the

right-hand side of the box has now been increased to $n_{r0} = 200$ cm^{-3}, to reduce the snowplough speed, so that the snowplough structure does not reach the right-hand side of the box and end the run prematurely. The scale l over which the B field falls away from 40 nT at the left-hand side to zero at the right-hand side is also unchanged. In all cases here the incident $T_p = 300$ eV, $T_e = 20$ eV, with a bulk flow speed of 350 km s^{-1}, representative of conditions seen at the IRM just prior to the release. The incident flow conditions are varied from sub- to supermagnetosonic by simply varying the incident proton number density, from 7.9–20 cm^{-3}, which spans the $\sim$10–15 cm^{-3} seen at the IRM.

3.2.1. *Supermagnetosonic.* The above parameters, with $n_p = 20$ cm^{-3} give $v_{MS} = 294.2$ km s^{-1} and $v_A = 195.8$ km s^{-1} so that in the rest frame of the release $M_{MS} = 1.19$. The upstream $\beta_p \simeq 1$ and $\beta_e \simeq 0.057$. The mean thermal speed of the incident ions $v_{th} = \sqrt{2kT/m} \simeq 240$ km s^{-1} gives a gyroradius of $\sim$60 km in the upstream 40 nT field, so that protons in the wings of the oncoming distribution will have gyroradii approaching the $\sim$ few hundred kilometres dimension of a Ba^+ release. We hence cannot remove the reflecting–gyrating ions simply on the basis of their $\hat{\mathbf{y}}$ transverse displacement, as was done in the case of the solar wind release, without also removing a significant fraction of the incident population. We will first examine results of a simulation for which no particles are removed, to determine a criterion for selectively removing the reflecting–gyrating population.

The bulk parameters of this simulation run are shown in Fig. 5, which is a plot of the structure that has evolved after $\sim$2.85 s. The top panel again shows the release and proton densities (the latter now scaled up by a factor of 10). The snowplough release ion population can be clearly seen at the right, at $x \simeq 1380$ km. Upstream (or to the left) of this, the proton number density first increases at $x \simeq 700$ km, the location of the upstream boundary, its value downstream of this location being on average approximately double the upstream value. In the next panel, which shows the magnetic, ion and electron pressures, we can see that unlike the solar wind case the ion pressure has increased dramatically (i.e. by a factor of about 8) downstream of the upstream boundary, and remains greater than or equal to the magnetic pressure. The electron pressure remains comparatively small, only dominating in the region just upstream of the snowplough release ions, where the ion pressure is reduced. In the vicinity of the snowplough boundary, i.e. at $x > 1300$ km, the bulk parameters exhibit the same behaviour as at the snowplough boundary in the solar wind release, that is, with the electron pressure dominating the ion pressure, and peaking at the cavity edge, just downstream of the magnetic pressure maximum. The phase space plots (bottom panel, Fig. 6) also show release ion kinetics similar to the solar wind release, except that now a more distinct population moving downstream of the snowplough, at $v \simeq 100$ km s^{-1}, is evident.

If the snowplough boundary operates in the same manner here as in the solar wind results, the potential jump at the boundary $\Delta\phi_{sp}$ should be just that required to accelerate the snowplough release ions. From the plot of the potential (next panel) we find $\Delta\phi_{sp} \simeq 100$ V. This compares favourably with the constant snowplough speed of 53 km s^{-1} found in the simulation results (which translates to a kinetic energy of $\simeq$102 eV for $m = 7$ ions). We can also compare this with the snowplough speed that would be predicted from the simple snowplough equation of motion (Chapman and Schwartz, 1987). If the snowplough structure is moving in a region of constant release ion number density, as is the case here, the snowplough speed is given by:

$$v_{sp} = \frac{\alpha}{1+\alpha} v_u$$

$$\alpha \simeq \left(\frac{n_u m_p}{n_R(x_{sp}) m_R} \right)^{1/2}. \tag{14}$$

This yields a snowplough speed of $\sim$38 km s^{-1}.

Turning now to the upstream boundary, we find that there are several differences between what is seen here, and what was found for the solar wind case. The upstream boundary layer has moved a considerable distance upstream in the 2.85 s of this run. Since formation (i.e. after $\sim$1 s) the boundary is $\sim$150 km in thickness, as opposed to $\sim$10 km in the solar wind results, with a downstream region that is dominated by the ion and magnetic pressures. "Wavelike" structures can be seen in the proton density, magnetic and electron pressures, potential and currents, in the region just downstream of the upstream boundary layer.

These features are all closely correlated with the ion kinetics, shown in detail in Fig. 6. The left- and right-hand columns, respectively, show the x and y velocity components of individual computational particles, plotted vs distance along the computational box, x. At the top of each column the electron, ion and magnetic pressures are shown to facilitate a comparison with the bulk parameters. The entire release ion population is plotted on single panels, the protons divided

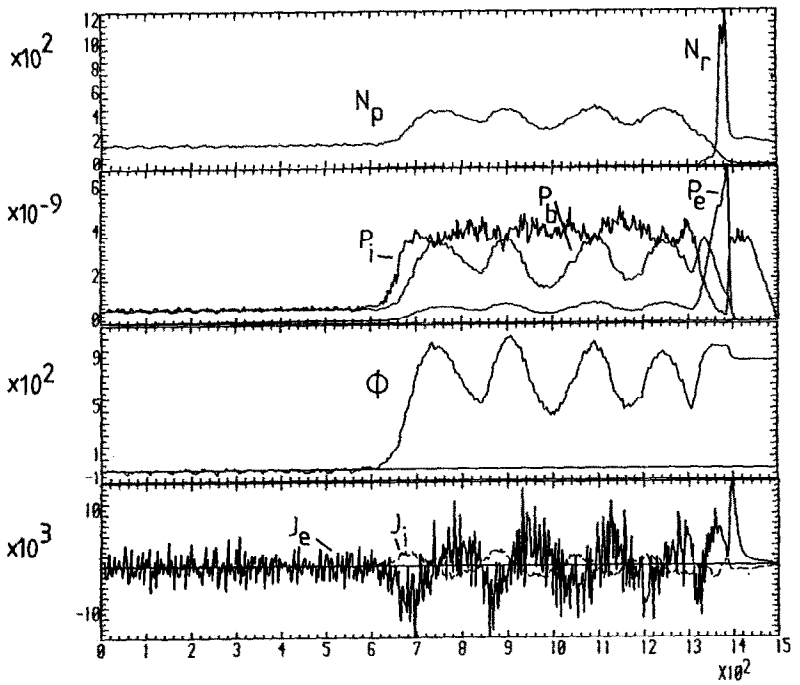

FIG. 5. A PLOT OF THE BULK PARAMETERS SHOWING THE STEADY STATE STRUCTURE THAT EVOLVES AFTER A RELEASE IN THE SUPERMAGNETOSONIC MAGNETOSHEATH FLOW.

From top to bottom the plot shows the proton and release ion number densities (N_p multiplied by a factor of 10), the ion, electron and magnetic pressures, the potential and the ion and electron contributions to the current, all plotted vs distance along the box x. All quantities are expressed in SI units. No computational particles were removed from the simulation.

according to their initial thermal speeds. The behaviour of the protons is then what might be expected at a supercritical shock interaction. Particles from the core of the incident distribution, which initially have low thermal speeds are shown in the upper panels. These are slowed on interacting with the upstream boundary layer, but transmitted without significant thermalization. This population as a whole executes serpentine motion in phase space in the wavelike field structure downstream. This behaviour changes as we move down the plot, and particles begin to reflect off the boundary layer, to gyrate in the upstream field and then to return to be transmitted to the downstream region. As in the case of a supercritical shock (e.g. Schwartz *et al.*, 1983) these reflecting–gyrating ions return to the boundary layer at a different point in velocity space, and in the downstream region gyrate at higher velocities about the population which was transmitted on first interacting with the boundary layer. The reflecting–gyrating ions form an increasingly significant part of the population as we move down the plot to increasing incident thermal energies. Any criterion used to remove the reflecting–gyrating population which may "miss" the release ion cloud must therefore act on those particles that originate from the wings of the incident distribution only, without disturbing the incident population upstream.

From Fig. 6 it is clear that the scale length of the rise in the bulk parameters at the upstream boundary, and the wavelike structures just correspond to the length scale associated with the motion of the reflecting–gyrating ions. The increase in ion pressure across this boundary is due to a large extent to the presence of the distinct populations of the reflecting–gyrating ions and the unthermalized transmitted low thermal speed core of the incident distribution [e.g. see equation (4)].

One further point of interest concerns the behaviour of the release ions, which remain in a region far downstream of the upstream boundary layer. This may have important consequences when we consider global momentum transfer, in which these ions may play a major role (e.g. Chapman, 1989; Haerendel *et al.*, 1986).

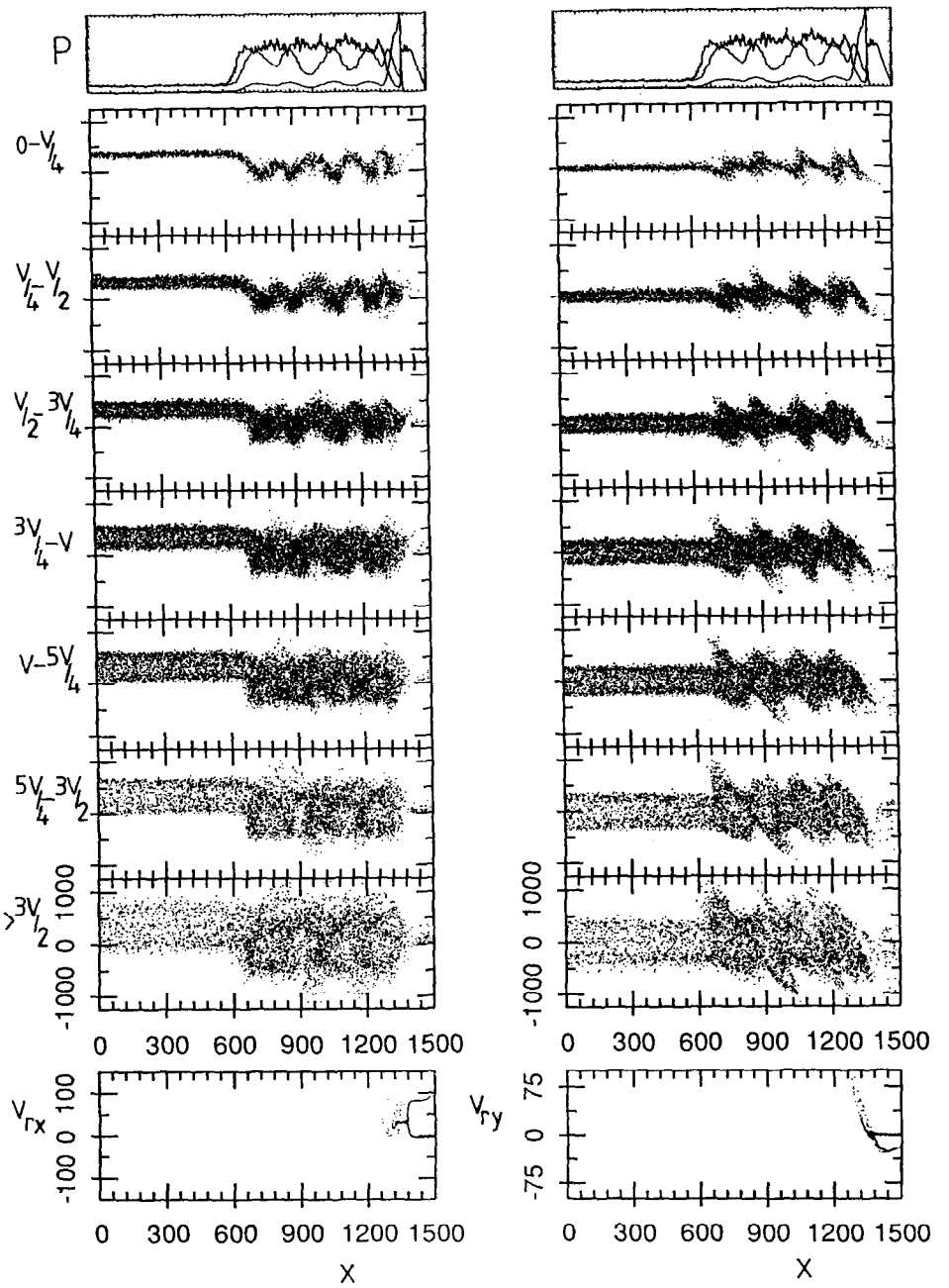

FIG. 6. THE LOCATIONS OF THE COMPUTATIONAL PARTICLES IN PHASE SPACE ARE SHOWN FOR THE SIMULATION RESULTS OF FIG. 5 (FOR A RELEASE IN THE SUPERMAGNETOSONIC MAGNETOSHEATH FLOW).
The left-hand set of panels show the particle v_x vs x, the right-hand set, v_y vs x. The top panel shows the electron, ion and magnetic pressures, for the purpose of comparison. The next seven panels show the locations of the computational particles representing the protons. These particles have been divided according to their incident thermal speed, with which they were injected into the computational box. Incident thermal speed increases as we move down the plot, so that the core of the incident population is shown at the top, and the high temperature wings towards the bottom. The bottom panel shows the entire release ion population. All quantities are expressed in SI units.

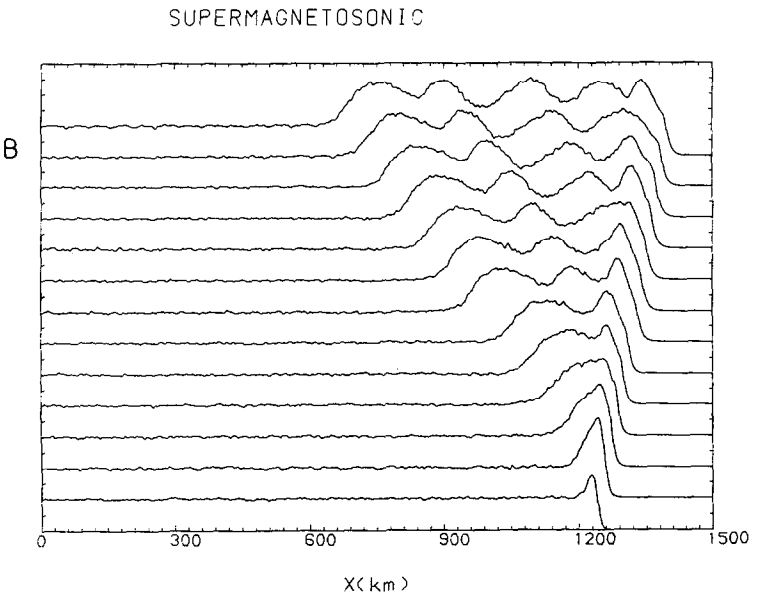

FIG. 7. THE MAGNETIC FIELD MAGNITUDE IS SHOWN PLOTTED VS DISTANCE ALONG THE COMPUTATIONAL BOX x FOR A SEQUENCE OF TIMES $\simeq 0.2$ S APART, STARTING AT $t \simeq 0.2$ S AND INCREASING AS WE MOVE UP THE PLOT.
These results are for the simulation run shown in Figs 5 and 6, representing a release in the supermagnetosonic magnetosheath flow, no particles having been removed from the simulation.

As the release ions are no longer in the vicinity of the upstream boundary layer, and there is no sink of protons, the conserved quantities given by equations (10)–(13) should be constant across the boundary layer, in the frame in which it is at rest. The behaviour of the upstream boundary layer over the entire simulation run is shown in Fig. 7, a plot of the magnetic field profile for a sequence of times $\simeq 0.2$ s apart. Soon after formation (i.e. after the first 1–1.2 s) both the snowplough and upstream boundary layers move apart at a constant speed, the upstream boundary layer propagating to the left at a speed $w \simeq -200$ km s^{-1}. Transforming to a frame moving at this speed, the conserved quantities given by equations (10)–(13) have been calculated for the time for which the bulk parameters are plotted in Fig. 5, and are shown in Fig. 8. In this moving frame all quantities are then on average conserved across the upstream boundary, and into the downstream region, only varying strongly in the vicinity of the release ions and snowplough structure.

We now assume that the protons can approximately be treated as a single fluid, in order to use the Rankine Hugoniot jump conditions [i.e. (10)–(13)] to deduce the speed of the upstream boundary w in the simulation rest frame. The jump conditions give, for example,

$$\frac{v_d}{v_u} = \frac{\left(1+\frac{3}{M_{MS}^2}-\frac{1}{2M_A^2}\right) \pm \left(\left(1+\frac{3}{M_{MS}^2}-\frac{1}{2M_A^2}\right)^2+\frac{8}{M_A^2}\right)^{1/2}}{8} \tag{15}$$

where all quantities refer to the moving frame. In the rest frame of the simulation, v_u is known and $v_d \simeq v_{sp}$, the snowplough speed, which may to a good approximation be estimated from the known release parameters using the simple snowplough equations of motion [e.g. equation (14)]. Substituting $v_u - w$ and $v_d - w$ in (15) for the upstream and downstream speeds in the moving frame, and solving for w in terms of the simulation (release) rest frame parameters gives:

$$w = \frac{(v_u+2v_d)}{3} \pm (\tfrac{4}{9}(v_u-v_d)^2+v_{MS}^2)^{1/2}. \tag{16}$$

With $v_d \simeq v_{sp} = 53$ km s^{-1} this gives $w \simeq -203$ km s^{-1} which compares favourably with the simulation results. In its rest frame, the boundary layer is an $M_{MS} = 1.88$ transition. Using the simple snowplough equation of motion (14) to estimate v_{sp} does not introduce a substantial error, giving $w = -218$ km s^{-1}.

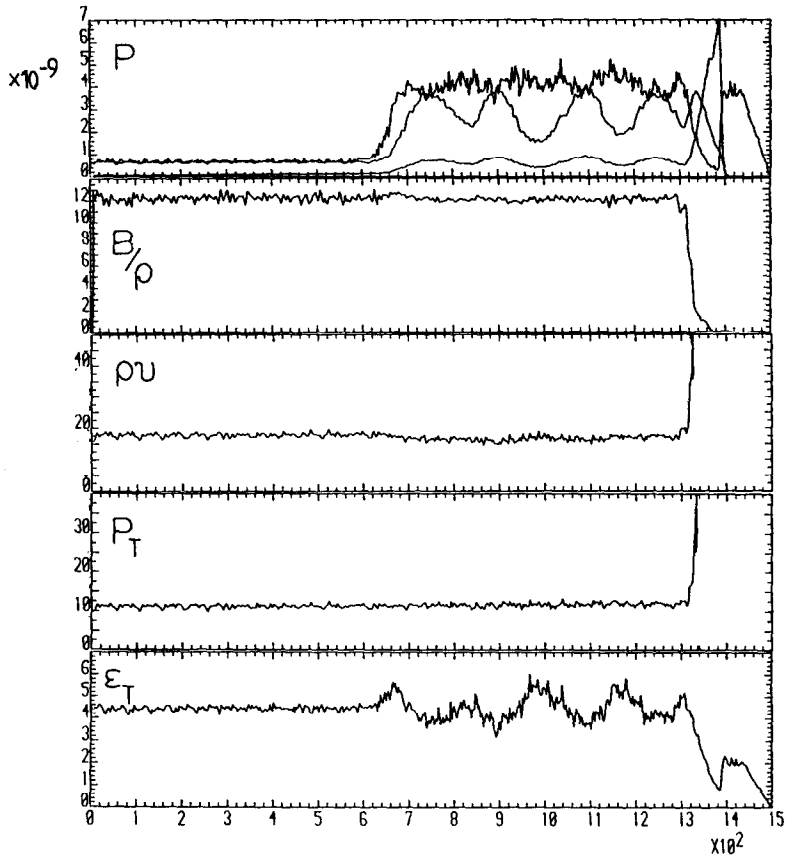

FIG. 8. THE "CONSERVED QUANTITIES" B/ρ, M_T, P_T AND ε_T (DEFINED IN THE TEXT) ARE SHOWN PLOTTED VS DISTANCE ALONG THE COMPUTATIONAL BOX x FOR THE CASE OF A RELEASE IN THE SUPERMAGNETOSONIC MAGNETOSHEATH FLOW (NO PARTICLES HAVING BEEN REMOVED FROM THE SIMULATION) SHOWN IN FIGS 5 AND 6. The top panel shows the electron, magnetic and ion pressures, enabling the location of the upstream and snowplough boundaries to be identified. All quantities are normalized except the pressures.

Conservation of the quantities given by (10)–(13) also implies that, once the rest frame of the boundary layer is known, the jump in the total pressure and number density can also be predicted. Effectively then, the snowplough structure that forms constrains conditions downstream of the upstream boundary layer, so that once a steady state evolves the propagation speed of the upstream boundary is also specified.

Finally, in the case of the solar wind it was found that the potential jump at the upstream boundary was approximately just that required to slow the oncoming proton flow. In Fig. 5 we see that $\Delta\phi_u \simeq 1000$ V. This must be compared with the kinetic energy change of the protons in the rest frame of the boundary, $\frac{1}{2}mv_u^2 - \frac{1}{2}mv_d^2 = 1230\,\text{eV}$ (where again v_u and v_d refer to the x-components of the proton velocity). The discrepancy between these is not surprising, since from Fig. 5 we can see that although $j_{iy} < j_{ey}$ it is not negligible at the upstream boundary.

These results then show the evolution of a steady state structure which when examined in terms of the bulk parameters and ion kinetics exhibits behaviour similar to that expected from a supercritical shock transition. As a consequence we are able to deduce analytically the jump in the bulk parameters that characterizes the upstream boundary layer, basically by means of the Rankine Hugoniot relations and the snowplough equation of motion (14). This would not be the case if the reflecting gyrating protons at the upstream boundary "miss" the release cloud, requiring a sink of particles in the simulation so that the quantities given by (10)–(13) are no longer conserved.

This possibility has been investigated by repeating the simulation run, removing the reflecting–gyrating ions. As an ion is reflected from the upstream boundary layer, the velocity with which it will subsequently gyrate in the local upstream magnetic field is initially mostly in the $-\hat{\mathbf{x}}$ direction. All protons with $v_x < -300$ km s^{-1} are removed from the simulation, as this corresponds to a gyroradius of >78 km in the upstream 40 nT field, and does not include the range of velocity space occupied by the incident distribution. About 23% of the protons incident in the frame moving with the upstream boundary layer are discarded by this criterion. This selection criterion for discarding particles from the simulation would, in the solar wind case, be identical to simply removing them on the basis of their y displacement as it can be seen from Fig. 2 that all of the particles that are reflected from the upstream boundary (to be ultimately discarded) have $v_x \sim -500$ km s$^{-1} \ll -300$ km s^{-1}.

The bulk parameters for this run (Fig. 9) show the situation after $t = 2.85$ s, that is, at the same time as for the previous results. On the right-hand side of the plot the snowplough boundary structure can be seen to have evolved as before, and is moving at the same speed downstream (to within ~ 1 km s^{-1}). This is consistent with the behaviour of the conserved quantities given by (10)–(13) where it is found that, whilst B/ρ and ρv vary, P_T is constant across the upstream boundary. The upstream boundary has once again moved upstream, but at a lower speed. This is evident in Fig. 10, a time sequence of the magnetic field profile in a format identical to Fig. 7. From the figure we can see that the upstream boundary has reached a quasi-steady configuration, with constant upstream speed $w = 113$ km s^{-1}. The boundary structure as a whole hence still evolves to occupy a large spatial region from early times, and if this is indicative of the spatial extent in the $\hat{\mathbf{y}}$ direction of the structure generated by the release clouds, then it is not appropriate to remove the reflecting–gyrating protons from the simulation, the previous results then providing a more accurate account of the early time release dynamics.

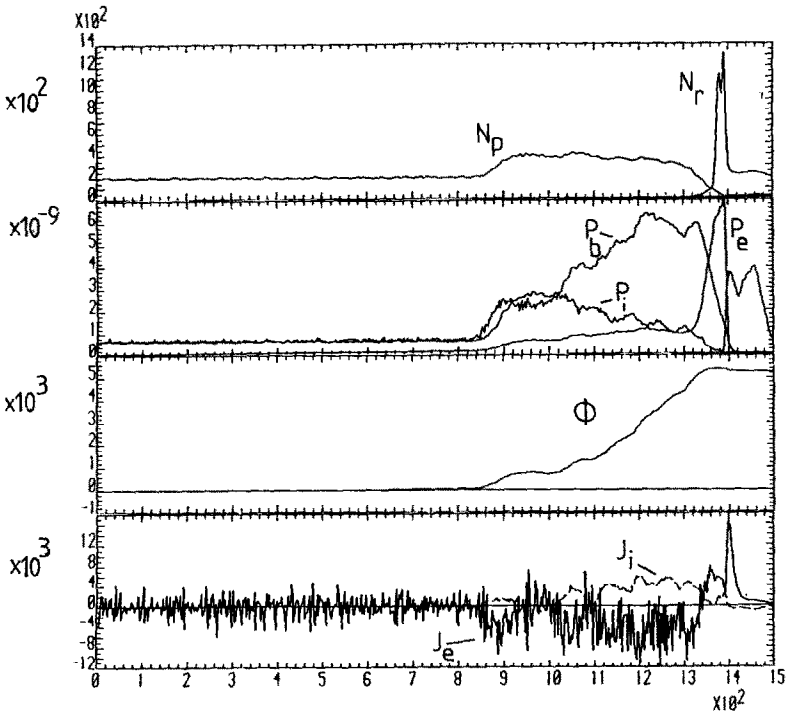

FIG. 9. A PLOT OF THE BULK PARAMETERS SHOWING THE STEADY STATE STRUCTURE THAT EVOLVES AFTER A RELEASE IN THE SUPERMAGNETOSONIC MAGNETOSHEATH FLOW.

From top to bottom the plot shows the proton and release ion number densities (N_p multiplied by a factor of 10), the ion, electron and magnetic pressures, the potential and the ion and electron contributions to the current, all plotted vs distance along the box x. All quantities are expressed in SI units. The reflecting–gyrating computational particles were removed from the simulation.

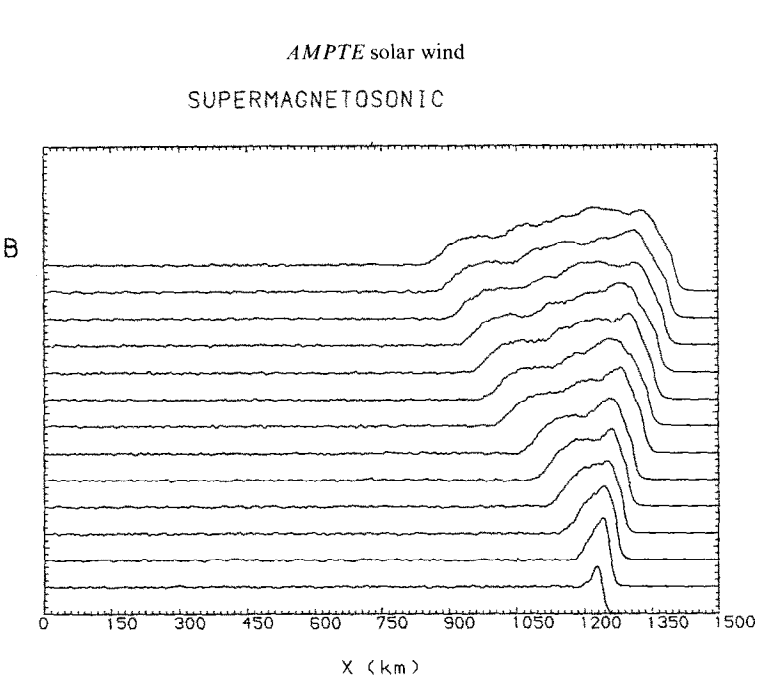

FIG. 10. THE MAGNETIC FIELD MAGNITUDE IS SHOWN PLOTTED VS DISTANCE ALONG THE COMPUTATIONAL BOX x FOR A SEQUENCE OF TIMES $\simeq 0.2$ S APART, STARTING AT $t \simeq 0.2$ S AND INCREASING AS WE MOVE UP THE PLOT.
These results are for the simulation run shown in Fig. 9, representing a release in the supermagnetosonic magnetosheath flow, the reflecting–gyrating particles having been removed from the simulation.

From Figs 9 and 10 it is clear that the "wavelike" structures that were associated with the reflecting–gyrating ions are no longer present, and the upstream boundary layer occupies a smaller spatial scale. Also, the ion pressure still increases across the upstream boundary layer, but is now dominated by the magnetic pressure downstream, consistent with the selective removal of the reflecting–gyrating proton population. The location of the computational particles in phase space is shown in Fig. 11, in the same format as Fig. 6. This plot gives a picture in phase space of the effect of the selection criterion that was chosen for removing the reflecting–gyrating proton population. In the upper panels of the figure we can see that particles originating from the core of the incident distribution are on average unaffected, although the population as a whole no longer executes serpentine motion in phase space due to the now smoother magnetic profile downstream. Moving further down the plot, most of the reflecting–gyrating particles can be seen to have been removed from the downstream population. The sink of particles therefore becomes progressively more significant as we move to higher incident thermal speeds, where the population comprises an increasingly larger proportion of the reflecting–gyrating population. Throughout the plot, the incident population can be seen to be unchanged, as required. This is presented more quantitatively in Fig. 12, which shows a histogram of the computational particles that have been removed from the simulation, binned according to their incident thermal speeds (i.e. in the same format as Fig. 3). The plot shows clearly the extent to which the population that has been removed from the simulation is skewed towards high incident thermal energies. This behaviour is just what would be expected of the reflecting–gyrating population, which has been shown both here for the releases, and for the case of a supercritical shock transition (Burgess *et al.*, 1989) to originate from the wings of the incident population.

The implication is then that, even when the reflecting particles are removed from the simulation, the upstream boundary layer that forms is still sufficiently "shock-like" to reflect a proportion of the incident population that originated principally from the wings of the incident distribution. We have seen however that, even when the reflecting–gyrating population is removed, the upstream boundary layer still propagates upstream at over ~ 100 km s^{-1}. This may suggest that the full 3-D structure generated by the release is, at early times, on sufficiently large scales that the reflecting–gyrating population do not "miss" the

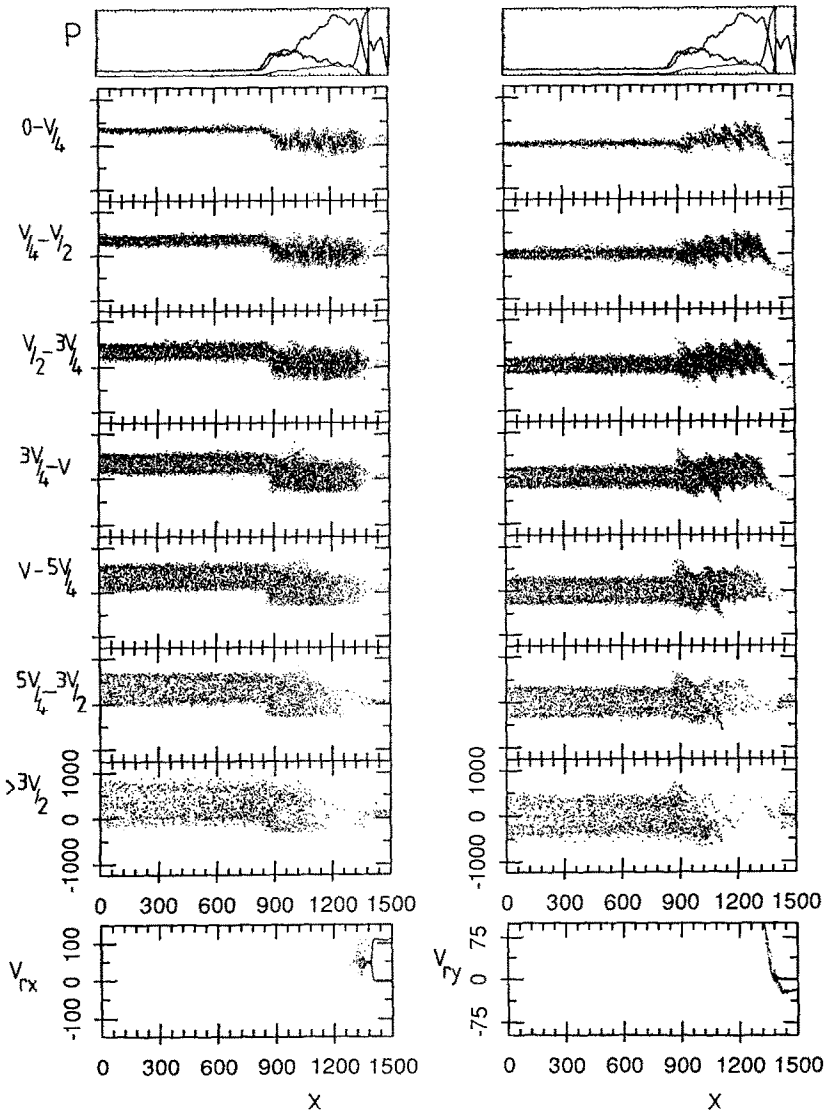

FIG. 11. THE LOCATIONS OF THE COMPUTATIONAL PARTICLES IN PHASE SPACE ARE SHOWN FOR THE SIMULATION RESULTS OF FIG. 9 (FOR A RELEASE IN THE SUPERMAGNETOSONIC MAGNETOSHEATH FLOW, THE REFLECTING–GYRATING PARTICLES HAVING BEEN REMOVED FROM THE SIMULATION).
The format is the same as for Fig. 6.

upstream boundary, so that the appropriate solution is closer to that when no particles are removed from the simulation.

3.2.2. *Submagnetosonic.* The previous simulation runs were repeated for the same parameters, except now with $n_p = 7.9\ \text{cm}^{-3}$, giving $v_A \simeq 312\ \text{km s}^{-1}$ and $v_{MS} \simeq 381\ \text{km s}^{-1}$, so that in the release (and simulation) rest frame $M_{MS} \simeq 0.92$. The upstream $\beta_p \simeq 0.4$, $\beta_e \simeq 0.026$.

The bulk parameters and phase space plots are shown in Figs 13 and 14, at a time $t \simeq 3.24$ s for a simulation run in which no particles have been removed. From these plots it is immediately apparent that the overall behaviour is the same as was found for the supermagnetosonic case. At the downstream end of the box, the snowplough structure has formed as before, moving to the right at $v_{sp} \simeq 44\ \text{km s}^{-1}$. The snowplough equation of motion (14), however yields $v_{sp} \simeq 25\ \text{km s}^{-1}$, and is now only in agreement within a factor of 2.

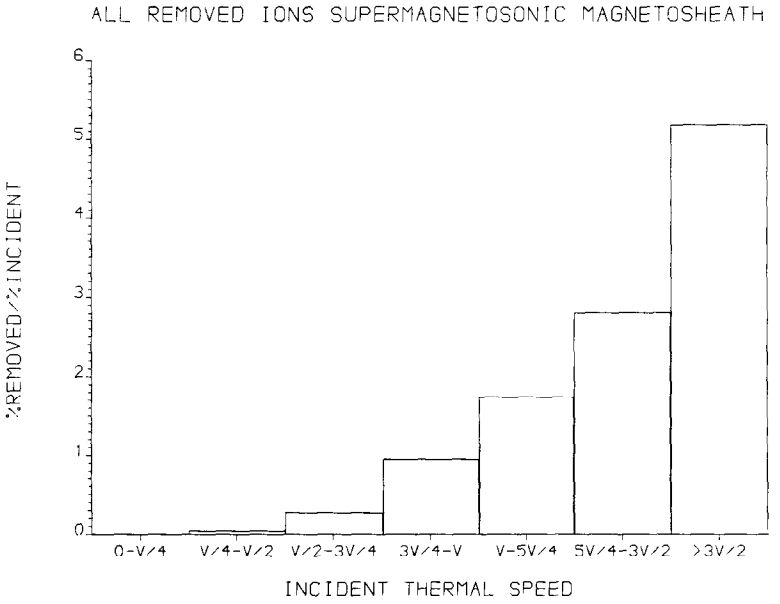

FIG. 12. THE REFLECTING–GYRATING COMPUTATIONAL PARTICLES FROM THE 'SUPERMAGNETOSONIC MAGNETOSHEATH RELEASE SIMULATION (e.g. FIG. 9) ARE BINNED ACCORDING TO THEIR INITIAL THERMAL SPEEDS WITH WHICH THEY ENTER THE COMPUTATIONAL BOX.
The range of each bin is expressed in terms of the thermal speed associated with the temperature of the initial distribution. The number of reflecting–gyrating computational particles in each bin is expressed as a percentage of the total number reflected, which has then been normalized to the percentage of the initial distribution lying in each bin.

The upstream boundary layer has propagated a substantial distance to the left of the box, and after formation moves at a constant speed $w \simeq -280$ km s^{-1} giving an $M_{MS} \simeq 1.65$ transition, in good agreement with $w = -286$ km s^{-1} found from equation (16) (i.e. basically from applying the Rankine Hugoniot jump conditions). This is not surprising since the conserved quantities given by (10)–(13) are found to be constant on average across the boundary layer to the same extent as in the supermagnetosonic case (calculated in the frame moving at $w = -280$ km s^{-1}). The magnetic pressure is now more than double the ion pressure downstream of the upstream boundary layer simply as a consequence of the smaller upstream plasma β_p. Again the electron pressure remains small throughout the region upstream of the snowplough boundary structure, in comparison with the magnetic and ion pressures, only dominating in the vicinity of the snowplough.

From the plot of the currents it appears that the ion contribution is still small compared with the electron contribution, but is not negligible. The loss of energy to the protons that are transmitted through the upstream boundary layer $(\frac{1}{2}mv_u^2 - \frac{1}{2}mv_d^2) \simeq 1512$ eV, when calculated in the frame moving with the boundary, is hence comparable with, but not exactly given by, the size of the potential jump $\Delta\phi_u \simeq 1600$ V.

Finally, the ion kinetics shown in Fig. 14, exhibit behaviour almost identical to that seen in the supermagnetosonic case. The core of the incident distribution is transmitted directly through the upstream boundary layer without significant thermalization, whereas a large proportion of ions originating from the wings of the incident distribution are reflected to gyrate in the upstream magnetic field to form a distinct gyrating population downstream. The same procedure has been followed as for the supermagnetosonic case to repeat this simulation run removing the reflecting–gyrating ions. The results of this run were qualitatively similar in all respects to the corresponding simulation with supermagnetosonic upstream parameters in which the reflecting–gyrating particles were discarded. The reflecting–gyrating ions were again successfully removed from the simulation without disturbing the initial population or the core of the incident distribution. The initial thermal speeds of the computational particles removed from the simulation are displayed in the histogram in Fig. 15,

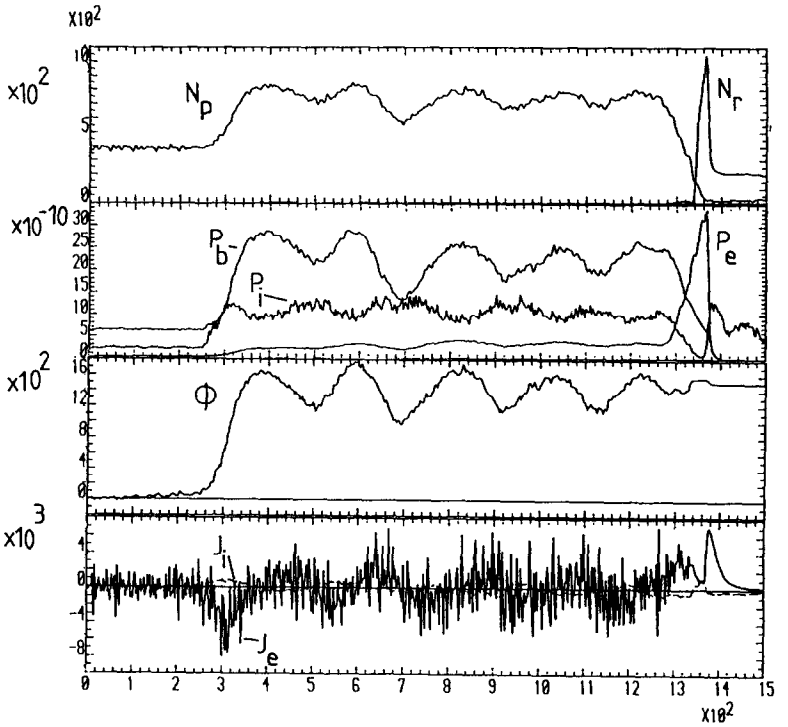

FIG. 13. A PLOT OF THE BULK PARAMETERS SHOWING THE STEADY STATE STRUCTURE THAT EVOLVES AFTER A RELEASE IN THE SUBMAGNETOSONIC MAGNETOSHEATH FLOW.
From top to bottom the plot shows the proton and release ion number densities (N_p multiplied by a factor of 50), the ion, electron and magnetic pressures, the potential and the ion and electron contributions to the current, all plotted vs distance along the box x. All quantities are expressed in SI units. No computational particles were removed from the simulation.

in the same format as before, and again we see that the majority of this population originated from the high thermal velocity wings of the incident distribution. Furthermore, in this simulation run the upstream boundary layer was found to propagate upstream at a significant velocity, i.e. $w \simeq 201$ km s^{-1}. The implication again may be that the structure generated by the release is, at early times, best described by the simulation results for which there was no sink of particles.

One further point of interest is that these results, appropriate for the submagnetosonic case, produce shock-like transitions which are in the subcritical regime [i.e. $M_{MS} \simeq 1.65$ compared with $M_{crit} \simeq 2.15$ for a $\beta \simeq 0.4$ transition (Edmiston and Kennel, 1984)]. The behaviour seen here hence is similar for both super- and sub-critical shocklike transitions.

4. CONCLUSIONS

The boundary layer structures that form at early times upstream of a release in the solar wind and magnetosheath flow have been examined in detail using 1-D hybrid simulations. This work is an extension of a previous study of the solar wind releases (Chapman and Schwartz, 1987) and is also the first investigation appropriate for magnetosheath conditions.

Just upstream of the release ion cloud and associated diamagnetic cavity a region of enhanced magnetic field forms, bounded on either side by relatively small scale boundary structures. On the downstream side, at the cavity edge, is a region where the electron pressure is enhanced and, along with the magnetic pressure, acts to accelerate the release ions within the vicinity. These release ions are gathered up "en masse" by a snowplough type process and move downstream with the same speed as the accompanying field structures.

On the upstream side, the jump in the magnetic (and in the solar wind case, electron) pressure acts to decelerate the oncoming protons to approximately the snowplough speed. The entire structure acts in this way to transfer longitudinal momentum between the

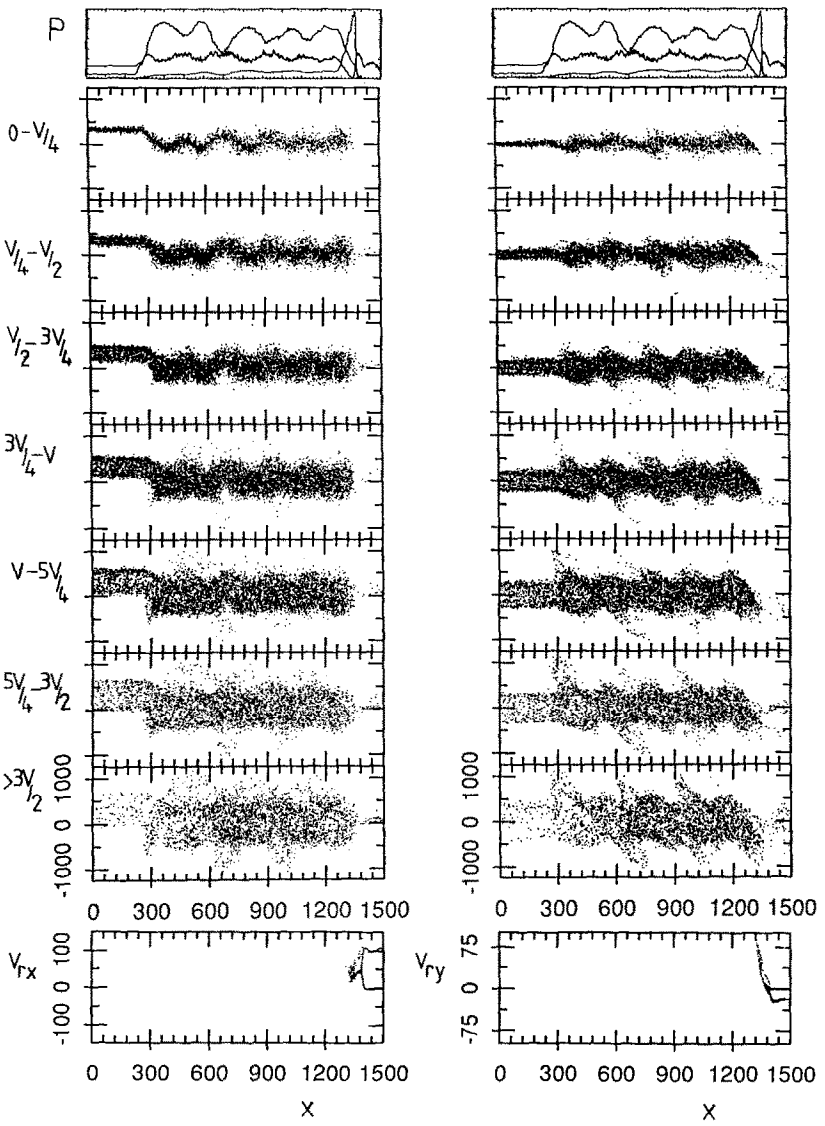

FIG. 14. THE LOCATIONS OF THE COMPUTATIONAL PARTICLES IN PHASE SPACE ARE SHOWN FOR THE SIMULATION RESULTS OF FIG. 14 (FOR A RELEASE IN THE SUBMAGNETOSONIC MAGNETOSHEATH FLOW, NO PARTICLES HAVING BEEN REMOVED FROM THE SIMULATION).
The format is the same as for Fig. 6.

oncoming protons and snowploughed release ions.

In both the solar wind and magnetosheath release simulations the snowplough boundary layer is found to evolve at the cavity edge with almost identical structure and ion kinetics. The electron and magnetic pressures dominate the ion pressure in this region, regardless of their relative magnitudes in the incident flow. The potential jump at this boundary is just equivalent to the kinetic energy of the release ions moving at the snowplough speed. The simple snowplough equation of motion predicts the speed of the snowplough boundary accurately for the case of a release in the solar wind, and to within a factor of 2 for the case of a magnetosheath release.

The properties of the upstream boundary layer differ between the solar wind and magnetosheath events. However, the underlying ion kinetics are similar in that a fraction of the incident proton population

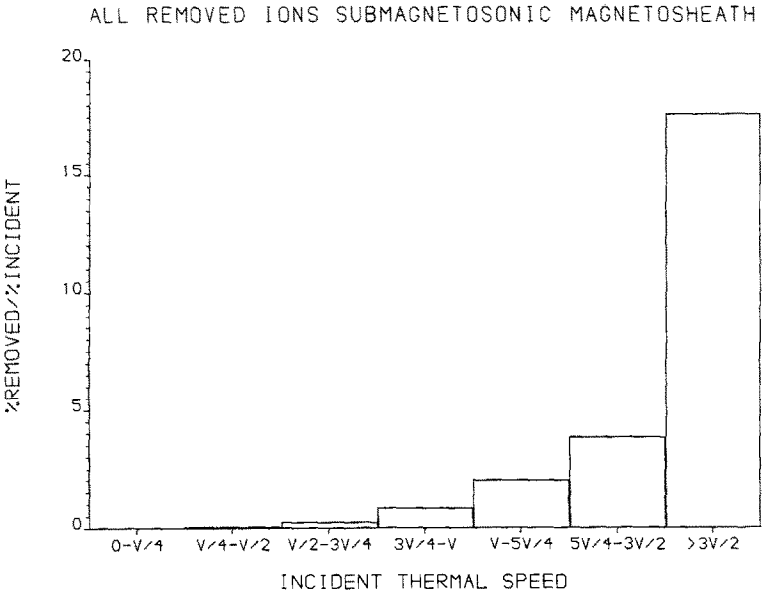

FIG. 15. THE REFLECTING–GYRATING COMPUTATIONAL PARTICLES FROM A SUBMAGNETOSONIC MAGNETOSHEATH RELEASE SIMULATION (NOT SHOWN) ARE BINNED ACCORDING TO THEIR INITIAL THERMAL SPEEDS WITH WHICH THEY ENTER THE COMPUTATIONAL BOX.

The range of each bin is expressed in terms of the thermal speed associated with the temperature of the initial distribution. The number of reflecting–gyrating computational particles in each bin is expressed as a percentage of the total number reflected, which has then been normalized to the percentage of the initial distribution lying in each bin.

is reflected at the upstream boundary layer in all cases. If the boundary layer were truly 1-D (an infinite planar structure) the reflecting ions would gyrate in the upstream field to return to the boundary layer to ultimately be transmitted, but in a different region in velocity space to the rest of the incident population that was transmitted on its first encounter with the boundary layer. This process has already been recognized as playing an important role in the thermalization at quasiperpendicular, supercritical shock transitions.

In the case of a solar wind release, the transverse displacement of the reflecting ions as they gyrate in the upstream magnetic field is considerably larger than the release cloud size, so that they cannot return to interact with the upstream boundary layer a second time. This is modelled by removing the reflecting–gyrating ions from the simulation. The upstream boundary layer that forms is quasi-steady, on a small ($\sim$ tens of kilometres) spatial scale and approximately at rest in the frame of the simulation (release). Mass and energy flux are not conserved across the boundary layer (and hence Rankine Hugoniot relations do not hold). The ion pressure drops as we move across the boundary layer into the downstream region, where the flow speed has slowed to approximately the snowplough speed.

In the case of both a solar wind or a magnetosheath release it is found that the protons that are reflected from the upstream boundary layer originate from the wings of the incident distribution, whether or not they are subsequently removed from the simulation. This behaviour has already been found in simulation studies of quasiperpendicular, supercritical shock transitions.

In the case of a magnetosheath release, it is found that, whether or not the reflecting–gyrating population is removed from the simulation, the upstream boundary layer moves upstream at a speed of a few hundred kilometres per second. This may suggest that the structure generated by the release, at least at early times, is larger than the transverse distance travelled by the reflecting–gyrating ions, and it is appropriate to retain them in the simulation. Rankine Hugoniot relations then apply across the upstream boundary layer in its rest frame. This leads to an expression for the speed w at which the upstream boundary moves upstream in terms of the flow speeds upstream and downstream of the boundary, the latter being just approximately the snowplough speed. Since the snow-

plough speed is approximately known from the snowplough equations of motion we can in principle determine w analytically from the release and incident flow parameters. Once the rest frame of the upstream boundary layer is known, Rankine Hugoniot relations then determine the jump in the magnetic field and the total (ion + electron) pressure, the latter being found from the simulation results to be dominated by the ion pressure for typical magnetosheath parameters. The increase in ion pressure in the compression region is to a large extent a result of the presence of the distinct population of reflecting–gyrating ions, as in the case of a supercritical shock transition.

Finally, we must consider whether or not the large spatial scales implied by the speed w at which the upstream boundary layer moves upstream realistically reflect what might be expected of the full 3-D structure generated by the magnetosheath release. In the case of submagnetosonic flow, the upstream propagating shock-like transition might represent the transient phase of a structure which eventually evolves into a laminar transition. The simulation results presented here would then be appropriate only at early times (i.e. for the first few seconds). On the other hand, if the oncoming flow is supermagnetosonic, a quasi-steady state could evolve in which a shock-like transition stands in the flow upstream of the release cloud. In this case, the structure and ion kinetics of this upstream boundary would not be dissimilar to those presented here. The standoff distance of this upstream boundary would then dictate the scale size of the perturbation to the flow, and hence whether the reflecting–gyrating ions were transmitted to the downstream region and if release ions were photoionized upstream in the oncoming flow. Due to the strong time dependence of the release interaction as a whole, it is not obvious that these quasi-steady structures would evolve and persist for the duration of the release interaction. However, evidence of the snowplough and upstream boundary layer structures is found in the *in situ* IRM observations of both the solar wind, and the (marginally supermagnetosonic) magnetosheath events (Dunlop, private communication, 1988).

Acknowledgements—Part of this work was performed whilst the author was supported by a SERC postdoctoral fellowship.

REFERENCES

Boyd, T. J. M. and Sanderson, J. J. (1969) *Plasma Dynamics*. Nelson, London, U.K.

Brecht, S. H. and Thomas, V. A. (1987) Three-dimensional simulation of an active magnetospheric release. *J. geophys. Res.* **92**, 2289.

Burgess, D., Wilkinson, W. P. and Schwartz, S. J. (1989) Ion distributions and thermalisation at perpendicular and oblique supercritical collisionless shocks. *J. geophys. Res.* (submitted).

Chapman, S. C. (1989) On the bulk motion of the ion clouds formed by the AMPTE solar wind/magnetosheath releases. *J. geophys. Res.* **94**, 227.

Chapman, S. C. and Dunlop, M. W. (1986) Ordering of momentum transfer along $\mathbf{V} \times \mathbf{B}$ in the AMPTE solar wind releases. *J. geophys. Res.* **91**, 8051.

Chapman, S. C. and Schwartz, S. J. (1987) One dimensional hybrid simulations of boundary layer processes in the AMPTE solar wind releases. *J. geophys. Res.* **92**, 11,059.

Cheng, A. F. (1987) Transverse deflection and dissipation of small plasma beams and clouds in magnetised media. *J. geophys. Res.* **92**, 55.

Dunlop, M. W., Chapman, S. C., Baumjohann, W. and Lühr, H. (1987) Boundary layer structures in the AMPTE solar wind releases (abstract). *EOS Trans. AGU* **68**, 1424.

Dunlop, M. W., Chapman, S. C. and Lühr, H. (1989) Boundary layer structures in the AMPTE solar wind releases: comparisons between 1D simulation results and IRM observations. *J. geophys. Res.* (submitted).

Edmiston, J. P. and Kennel, C. F. (1984) A parametric survey of the first critical Mach number for a fast MHD shock. *J. plasma Phys.* **32**, 429.

Haerendel, G., Paschmann, G., Baumjohann, W. and Carlson, C. W. (1986) Dynamics of the AMPTE artificial comet. *Nature* **320**, 720.

Krimigis, S. M., Haerendel, G., McEntire, R. W., Paschmann, G. and Bryant, D. A. (1982) The Active Magnetospheric Particle Tracer Explorers (AMPTE) program. *EOS Trans. AGU* **63**, 843.

Leroy, M. M. (1983) Structure of perpendicular shocks in collisionless plasma. *Phys. Fluids* **26**, 2742.

Lühr, H., Southwood, D. J., Klöcker, N., Acuña, M., Häusler, B., Dunlop, M. W., Mier-Jedrzejowicz, W. A. C., Rijnbeek, R. P. and Six, M. (1986a) *In situ* magnetic field measurements during AMPTE solar wind Li^+ releases. *J. geophys. Res.* **91**, 1261.

Lühr, H., Southwood, D. J., Klöcker, N., Dunlop, M. W., Mier-Jedrzejowicz, W. A. C., Rijnbeek, R. P., Six, M., Häusler, B. and Acuña, M. (1986b) *In situ* magnetic field observations of the AMPTE artificial comet. *Nature* **320**, 6064.

Lui, A. T. Y., Goodrich, C. C., Menkofsky, A. and Papadopoulos, K. (1986) Early time interaction of lithium ions with the solar wind in the AMPTE mission. *J. geophys. Res.* **91**, 1333.

Papadopoulos, K. and Lui, A. T. Y. (1986) On the initial motion of artificial comets in the *AMPTE* releases. *Geophys. Res. Lett.* **13**, 925.

Schwartz, S. J., Thomsen, M. F. and Gosling, J. T. (1983) Ions upstream of the earth's bow shock: a theoretical comparison of alternative source populations. *J. geophys. Res.* **88**, 2039.

Tidman, D. A. and Krall, N. A. (1971) *Shock Waves in Collisionless Plasmas*. Wiley-Interscience, New York.